ELSEVIER

Journal of Membrane Science 115 (1996) 49–63

journal of MEMBRANE SCIENCE

Influence of surface interaction on transfer during colloid ultrafiltration

P. Bacchin, P. Aimar *, V. Sanchez

URA CNRS de Génie Chimique, Laboratoire de Génie Chimique et Electrochimie, Université Paul Sabatier, 118 Route de Narbonne, 31062 Toulouse Cedex, France

Received 23 February 1995; revised 17 October 1995; accepted 18 October 1995

Abstract

Experimental ultrafiltration (UF) of clay suspensions having different salinity shows that the presence of salt affects the transfer mechanisms, such as deposition kinetics, hydraulic resistance of the deposit and salt retention by the deposit. Such changes are the results of the variation in surface repulsive interaction between particles with the salt concentration (DLVO theory). With respect to the deposition kinetics, it is observed that as salt concentration increases the critical flux decreases to zero; this coincides with the occurrence of an adhesion mechanism. These phenomena are modelled by considering transport by surface interaction of the particles near the surface. Variations in hydraulic resistance of the cake are explained through a modified Kozeny–Carman equation. A reduction in porosity due to a decrease in repulsive interaction and a particle size increase due to coagulation are involved. Salt retention is described by considering (i) electrostatic partition (ii) salt transport by convection and diffusion in the boundary layer and in the porous medium. Analysis of salt retention and of hydraulic resistance of the cake lead to the same conclusions about the deposit properties. An important result is that surface interactions (hence the suspension stability) are as important as operating conditions for the membrane processing of colloidal suspensions.

Keywords: Membrane processes; Fouling; Retention; Colloid; Stability

1. Introduction

Ultrafiltration is a pressure driven membrane process of importance to the separation and concentration of colloid suspensions, which include clay particles as well as proteins and other macromolecules. The field of application of such processes is expanding into water treatment, the dairy and pharmaceutical industry or in biotechnology. So far works on ultrafiltration of colloids have pointed out both theoretical and practical problems.

As reported by Belfort et al. [1], a lot of experimental works have shown that productivity and efficiency during colloid ultrafiltration depend on the physico-chemical properties of the suspension, such as pH or salinity. Theoretical works assume that this dependence is due to surface interaction between colloidal particles. Cohen and Probstein [2] state that only models taking physico-chemical properties of the suspension into account should explain the "colloidal flux anomaly". McDonogh et al. [3] show that

* Corresponding author.

SSDI 0376-7388(95)00279-0

surface interaction variations induce changes in the deposit permeability. On another hand, it has been known for a long time that solute retention is highly sensitive to surface interaction between membrane and solute [4].

The purpose of this paper is to detail and explain how electrostatic interactions affect mechanisms of (i) deposition kinetics, (ii) hydraulic resistance of the deposit and (iii) salt retention by the deposit during colloidal ultrafiltration. This work, investigating different mechanisms, is based on a set of experiments on clay suspensions under different ionic strengths (and then with different surface interactions). In the first section, the influence of salt concentration on ultrafiltration productivity is studied. Analysis of filtration results allows one to look into the two mechanisms involved in membrane fouling: the deposition kinetics and the hydraulic resistance of the deposit. In the second part, effects of surface interaction on process selectivity for inorganic salts are detailed through data on salt retention by the colloidal deposit. Theoretical models taking electrostatic interactions into account have been developed to describe the data.

2. Experimental setup and procedure

2.1. UF unit

The ultrafiltration setup is shown in Fig. 1. The permeate line is returned to the retentate tank after the measurement of the permeation flux, J. With such a configuration, the variation in concentration of particles in the retentate, dc/dt, measured by turbidimetry, allows the quantity of matter which disappears from the bulk (the amount deposited on the membrane) to be determined. pH and conductivity are measured on the retentate and permeate lines.

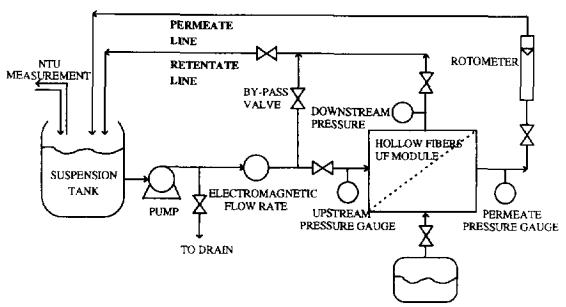

Fig. 1. Ultrafiltration experimental setup.

The ultrafiltration module contains 24 polysulfone outer skinned hollow fibers (1.02 mm external diameter) (Lyonnaise Des Eaux Dumez, Toulouse, France) with a nominal cutoff of 300 kDa (accordingly, clay used in these experimental studies was 100% rejected). Solutions were circulated (cross-flow filtration) along the external surface of the fibers in a module where the fibers were sufficiently spaced to be considered non interfering with each other from a mass transfer or a hydrodynamic point of view. The total membrane area is 0.024 m^2. The module has a hydraulic diameter of 17.7 mm [5]. The flow rate is 6.94×10^{-5} m^3/s (250 l/h) and corresponds to linear velocities of 88 mm/s (Reynolds numbers of the order of 1500). The mean boundary layer for this geometry is about 20 μm. The permeation velocity (permeate flux per unit membrane area) is 5×10^{-5} m/s under a pressure of 100 kPa.

2.2. Preparation and characterisation of suspensions

The colloid used was a clay: the bentonite. Bentonite particles are platelets, the larger dimensions of which are about one hundred times larger than the thickness. Their zeta potential, characterising the particle charge, is of the order of -40 mV [6]. A first suspension was prepared by dispersing 60 g of clay in 2 l of "osmosed" water. Four settlings, each 4 h long, lead to a suspension of 17 g/l consisting of micron sized colloidal particles. KCl was added in various quantities to this clay suspension diluted to 0.3 g/l 15 h before UF in order to obtain equilibrated suspensions of various stabilities. An important work of calibration of turbidity with different colloidal concentrations and with different salt concentrations has been made to derive the mass concentration from turbidity (in NTU) and conductivity. In the absence of salt addition, the conductivity of a 0.3 g/l bentonite suspension was equivalent to a 1×10^{-5} M KCl solution.

Particles size was measured with a laser light scattering apparatus (Coulter N4D). In "osmosed" water (10^{-5} M), the apparent size of the particles was 0.7 μm with a typical standard deviation of

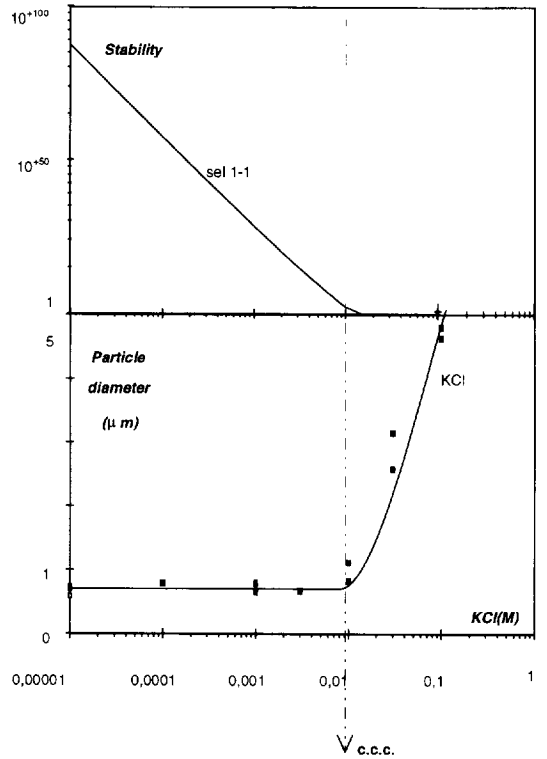

Fig. 2. Stability factor, W_c, and particle diameter, $2a$, of bentonite as a function of salt concentration.

25%. The variation in the mean size versus salt concentration is presented in Fig. 2. For low salt concentration (up to 10^{-2} M), the size was constant but for higher concentration an increase in apparent size was observed. The value of 10^{-2} M corresponds to the critical concentration of coagulation (ccc). The existence of the ccc is explained by the DLVO theory [7]. This theory states that the stability W_c of the suspension (corresponding to the ratio of rate of coagulation due to diffusion, N_c, to the actual rate of coagulation, N) is a function of the surface interaction between particles:

$$N = \frac{N_c}{W_c} \text{ with } W_c = 2a\int_{2a}^{\infty} e^{\frac{V}{kT}} \frac{dr}{r^2} \quad (1)$$

When the stability factor is close to 1 a rapid coagulation is observed whereas a stability factor larger than 10^5 means that repulsive interactions between particles prevent particles from coagulation and the suspension appears stable at the lab scale. As illustrated in Fig. 2, the calculation of the stability of the clay [8] used in the present work leads to determine a ccc close to the one deduced from experiments.

2.3. Methods

A preliminary experiment consists in a run performed in the unit without filtration ($\Delta P = 0$). This run allows the amount of clay disappeared by adhesion of colloids on the pipes, tank and other walls of the set-up to be determined. This adhesion reaction is described using a first order kinetics [9]:

$$\frac{dc}{dt} = Kc \quad (2)$$

where K is the apparent rate of adhesion.

Once this mechanism has been quantified, an ultrafiltration run is carried out with a fresh solution on the cleaned unit. Typical experiments cover a time period of 2 to 3 h with parameters measured every 10 min. The concentration reduction in the tank allows the deposited mass on the membrane, M_d, to be determined after substraction of the effect of adhesion:

$$\frac{Vol}{S}\left(\frac{dc}{dt} - Kc\right) = \frac{dM_d}{dt} \quad (3)$$

The permeation flux, J, and the mass deposited on the membrane, M_d, have been determined during ultrafiltrations performed at different values of salt concentration. Conductivity measurements in retentate and permeate lines allow the calculation of the retention, R, defined as:

$$R = 1 - \frac{c_p}{c_0} \quad (4)$$

where c_p and c_0 are the permeate and the retentate salt concentration respectively. A retention of 1 corresponds to a salt totally retained by the deposit.

3. Part I: Filtration mechanisms

In this section, filtration results are first presented and analysed in order to deduce the hydraulic resistance of the deposit and the parameters of deposition kinetics. Then, the variation in hydraulic resistance of the deposit is described as the combination of clay

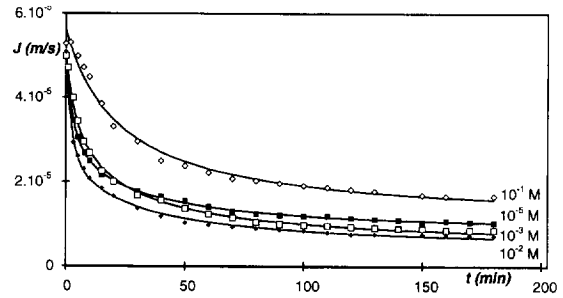

Fig. 3. Permeation velocity versus time for different salt concentrations.

size increase due to coagulation and of a porosity decrease linked to repulsive interaction changes. Then, deposition kinetics are explained considering the additional effect of migration induced by interaction on the transport phenomena in the boundary layer surrounding the deposit.

3.1. Filtration results and preliminary analysis

Figs. 3 and 4 represent the results of experiments, in terms of permeation flux through the membrane and deposited mass on the membrane respectively, with different salt concentrations in the suspension. Operating conditions are: a clay concentration of 0.3 g/l, a tangential flow rate of 6.94×10^{-2} l/s and a transmembrane pressure of 100 kPa. In Fig. 3, we note that a low concentration salt (10^{-2} M) induces a low flux whereas a high salt concentration (10^{-1} M) leads to a large flux as compared to the situation without salt added (equivalent to 10^{-5} M). On another hand, the deposited mass on the membrane monotonously increases with salt concentration (Fig. 4). No direct relationship between flux and deposited mass can be deduced. This problem leads to a first model [5] which considers fouling to be the combination of cake filtration [Eq. (5)] and deposition kinetics [Eq. (6)]:

$$J = \frac{\Delta P}{\mu(R_m + R_c)} = \frac{\Delta P}{\mu(R_m + \alpha M_d)} \tag{5}$$

$$N = \frac{dM_d}{dt} = Jc - n = (J - j_{crit})c \tag{6}$$

The cake filtration law describes the fouling resistance as the sum of the membrane hydraulic resistance, R_m, and of the cake resistance, R_c. The latter resistance is assumed proportional to the amount deposited on the membrane, M_d, and to the cake specific resistance, α. The rate of deposition to the interface is expressed as the amount brought by convection, Jc, minus a back flux, n. Eq. (6) introduces the idea of a back flux which is in opposition to convection. In the same way, it predicts a stationary flux, $j_{crit} = n/c$, for which this back flux is equal to the convection term, and $N = 0$.

According to these equations, experimental results (J and M_d) allow to the determination of two parameters from ultrafiltration runs: α the cake hydraulic resistance and j_{crit}. These parameters are nearly constant during filtration and their variations versus different salt concentrations and different applied pressures (filtration results for the different pressures not presented here) are shown in Figs. 5 and 6 and detailed in the two next paragraphs. Values for the adhesion constant, K, added in Fig. 6, are determined from preliminary experiments using Eq. (2).

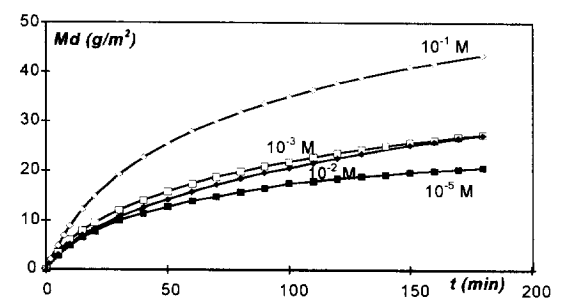

Fig. 4. Deposited mass versus time for different salt concentrations.

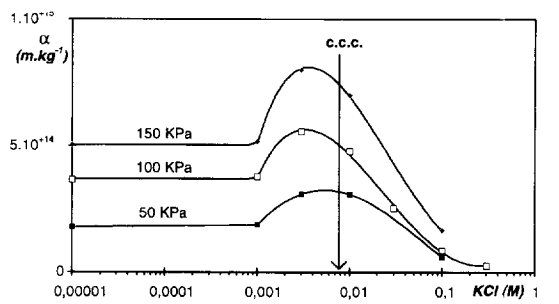

Fig. 5. Specific resistance of the colloid cake versus salt concentration.

3.2. Hydraulic resistance of the colloid deposit

Values of cake resistance in Fig. 5 show an important dependence on salt. The effect of pressure due to the compressibility of the cake seems not affected by the ionic strength. The average value for the compressibility here is 0.84 and is similar to those already determined for bentonite [5]. With salt concentration, one can note a first increase (about 30%) of the hydraulic resistance followed by an important decrease. The critical concentration for coagulation, ccc, seems to be the concentration for which the transition occurs. Then, the development of a model for hydraulic resistance, taking the particle size into account, seems necessary to describe the data.

3.2.1. Model

The flow through a porous medium is described by the Darcy law assuming that the flow, q, is produced by an applied pressure, ΔP_c (here only on the cake) per unity of deposit mass per unit area, M_d multiplied by a factor, $1/\mu\alpha$:

$$q = -\frac{1}{\mu\alpha}\frac{\Delta P_c}{M_d} \tag{7}$$

α is the specific hydraulic resistance of the cake in m kg^{-1}. It can be linked to the cake permeability defined (in m^2) considering that a relationship exists between the cake mass and its thickness, l:

$$M_d = \rho_s(1-\epsilon)l \tag{8}$$

where ρ_s is the density of a bentonite particle (of the order of 3). In our case, the porous medium is created by bentonite platelets the length and the width of which are one hundred times larger than the thickness, e. In such conditions, the medium can be modelled as a series of fissures of length, L, and depth, l, these being much larger than their thickness, d_i (Fig. 7). The porosity, ϵ, of such a packed geometry can be written as:

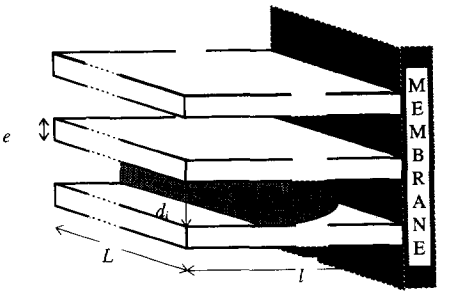

Fig. 7. Model used in this work to represent the porous medium constituted of bentonite platelets.

$$\epsilon = \frac{d_i}{d_i + e} \tag{9}$$

The flow through such a medium is $q = \bar{u}\epsilon$ where $\bar{u}$ is the mean velocity of a steady laminar flow between parallel planes. By analogy with Eq. (7), this leads to the following value for the specific resistance:

$$\alpha = \frac{12\epsilon}{\rho_s(1-\epsilon)}\frac{1}{d_i^2} \tag{10}$$

Substituting for d_i [Eq. (9)] in Eq. (10) gives:

$$\alpha = \frac{3(1-\epsilon)}{\epsilon^3\rho_s}\left(\frac{2}{e}\right)^2 \tag{11}$$

This equation allows to take into account two effects on the hydraulic resistance of the deposit: one of particle size through the thickness, e, and one of the porosity, ϵ. The platelets thickness, e, can be linked to a radius, a, of an equivalent spherical particle determined by light scattering measurements, by considering that platelets have the same volume as the sphere:

$$e = 3\sqrt{\frac{4\pi}{3\times 10^4}}\,a = 0.075a \tag{12}$$

This assumption is based on the fact that during size determination by laser light scattering technique the

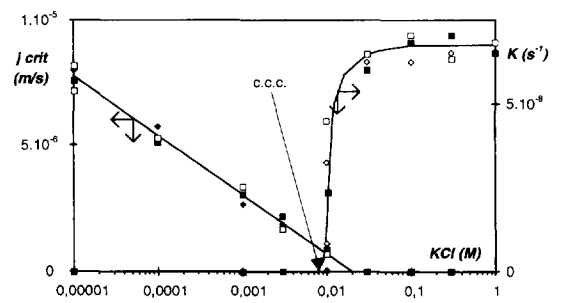

Fig. 6. Kinetics deposition parameters, j_{crit} and K, versus salt concentration (♦ = 50 kPa, □ = 100 kPa, ■ = 150 kPa).

measured parameter is the volume of particle. Here, it is interesting to note that Eq. (11) can be compared to those determined for a spherical packing by Kozeny–Carman if we include a shape correction factor, f:

$$\alpha = \frac{5(1-\epsilon)}{\epsilon^3 \rho_s}\left(f\frac{3}{a}\right)^2 \tag{13}$$

The shape factor can be defined for a single particle [10] as the ratio of the surface of the particle to the surface of a sphere having the same volume as the particle, and is of 9.09 in our platelet geometry.

The application of the model is performed according to the following procedure. The particle size, a, deduced from experimental measurements (Fig. 2) leads to the equivalent thickness of the particle, e, by Eq. (12). Application of Eq. (11) to experimental values of specific hydraulic resistance with data on the particle thickness allows the derivation of cake porosity. By applying the definition given in Eq. (9) for porosity, one can deduce the interparticle distance, d_i.

3.2.2. Discussion

The cake porosity, deduced from modelling, is plotted against salt concentration in Fig. 8. It appears that cake porosity is reduced when salt concentration increases. Variations in cake resistance with salt concentration deduced from experimental data (Fig. 5) are then the result of cake packing (Fig. 8) combined with an increase in the particle size due to coagulation (Fig. 2). The reduction in porosity can theoretically be explained in a simpler way by interpreting the results through the interparticle distance. As plotted in Fig. 9, the interparticle distance, d_i, first decreases when the salt concentration increases

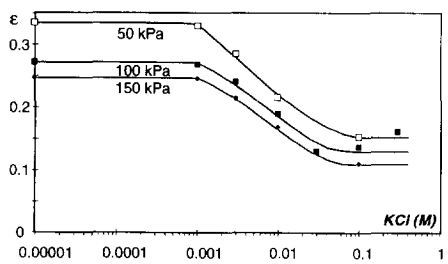

Fig. 8. Porosity of the colloidal deposit versus salt concentration deduced from modelling.

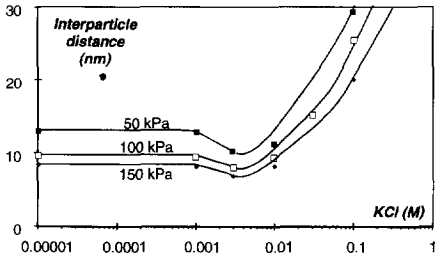

Fig. 9. Interparticle distance in the cake versus salt concentration.

as a consequence of the porosity reduction. It then increases because of an increase in size of particles making the deposit. The first decrease in interparticle distance with salt concentration can be described with a model based on a balance between the surface interactions and pressure drop through the cake as developed by McDonogh et al. [3]. It is assumed that the distance between particles is the one corresponding to a balance between an electrostatic repulsion pressure, p, and an applied pressure through the cake, ΔP:

$$d_{i0}/\Delta P = p = 2nkT(\cosh(u) - 1)$$

with

$$u = \frac{ze\Psi_d}{kT} = 8Y_0 \exp(-\kappa d_{i0}) \tag{14}$$

In a second step, the increase in the interparticle distance is explained by the fact that the distance is proportional to particle size if we consider that particle size has no effect on porosity [Eq. (9)]:

$$d_i = d_{i0}\frac{a}{a_{(I=0\,M)}} \tag{15}$$

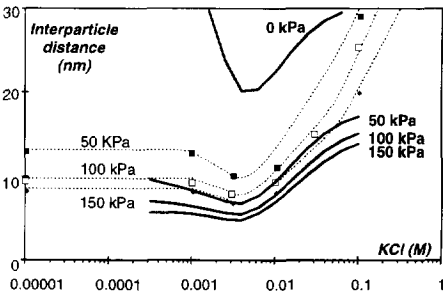

Fig. 10. Interparticle distance calculated from theoretical considerations (bold lines) compared to experimental deduced values (dashed lines and symbols).

Fig. 10 shows that calculated distances with Eqs. (14) and (15) are close to those deduced from experimental results. The calculation for a pressure of zero, made using the swelling distance for montmorillonite as determined by Norrish [11], seems to be in good agreement with these results. Surface interactions provide an explanation for the observed variations in specific resistance through two phenomena: (a) cake packing due to the reduction of interparticle distance in the cake caused by the repulsive interaction decrease between particles and (b) the coagulation of particles occurring when repulsive interactions become negligible.

3.3. Deposition kinetics analysis

As can be understood from Fig. 6, salt concentration in the suspension significantly affects the deposition mechanism whereas the applied pressure has a negligible effect. For low ionic strength there is a large limiting flux which controls the deposition on the membrane. Addition of salt results in a lower value of the limiting flux. For ionic strengths near the ccc, this limiting flux is nearly zero: the amount of matter deposited on the surface is equal to the amount brought by convection (dead-end filtration). Adhesion appears for salt concentration around the ccc. This rapid mechanism is often observed and allows the determination of a critical deposition salt concentration, cdc as proposed by van de Ven [12]. Such important changes in colloid mass transport with ionic strength leads one to consider the surface interactions between the particle approaching the fouled membrane surface and the particles already sitting on the membrane (Fig. 11).

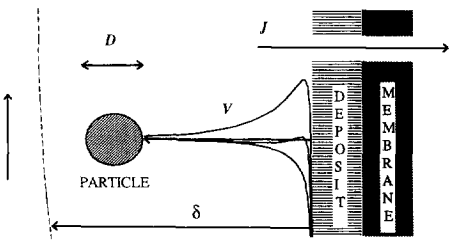

Fig. 11. Different transport mechanisms involved in the mass deposition.

3.3.1. Model

A model based on the continuity of the mass transport [Eq. (16)] and accounting for the transport of particles [Eq. (17)] in the boundary layer by convection (a), diffusion (b) and surface interaction enhanced migration (c) has been previously developed [8].

$$\nabla N = 0 \tag{16}$$

$$N = \underset{\text{(a)}}{Jc} \quad \underset{\text{(b)}}{-D\nabla c} \quad \underset{\text{(c)}}{-\frac{D}{kT}c\nabla V} \tag{17}$$

$$x = 0 \quad c = 0 \tag{18a}$$

$$x = \delta \quad c = c_0 \tag{18b}$$

The boundary conditions used to solve the continuity of mass transport across the boundary layer are the perfect sink on the deposit side [Eq. (18a)] and the typical boundary condition of the film model on the bulk side [Eq. (18b)]. Such a model is similar to those developed for deposition on a collector (non permeable surface) as summarised by Jia and Williams [13]. Integration leads to a mass transfer equation linking the rate of deposition, N, to convection, J, and to surface interaction, V (respectively Sh, Pe and W_d in a non-dimensional form):

$$Sh = \frac{1}{(W_d - 1)e^{-Pe} + \frac{1}{Pe}(1 - e^{-Pe})} \tag{19}$$

with

$$Pe = \frac{J\delta}{D}, \tag{19a}$$

$$Sh = \frac{N\delta}{Dc_0} \tag{19b}$$

and

$$W_d = \frac{\int_0^\delta e^{\frac{V}{kT}} dx}{\delta} \tag{19c}$$

The parameter, W_d, characterises the stability of a single particle with respect to the membrane. In the present case, we assume that at least a layer of particles is deposited on the membrane and then we consider the interaction of a sphere with a surface

having the same properties as the particles. This latter parameter can be linked to W_c, the stability factor for coagulation, defined in Eq. (1), as follows:

$$\frac{W_d - 1}{W_c - 1} = \frac{2a}{\delta} \tag{20}$$

W_d takes the cross-flow velocity through the boundary layer thickness into account: for a repulsive interaction an increase in velocity induces an increase in stability of the suspension with respect to the deposition. In our case, where boundary layer thickness is of the order of magnitude of the particle size, parameters W_d and W_c are numerically close to each other. It is not the case with a protein, the small size of which gives a value of W_c larger than W_d. This explains why proteins that are stable in solution (large W_c) may adsorb onto membrane surfaces (low W_d).

Simulation of colloidal fouling can be made using the mass transfer Eq. (19) combined with a filtration law [Eq. (5)]. Here only two limiting cases of Eq. (19) are necessary to explain the results presented in Fig. 6.

According to Eq. (19), for large values of the stability factor, $W_d \gg 1$, i.e. for strong repulsive interaction between particles, a critical Pe exists below which no deposition occurs [$N = 0$ in Eq. (6)] and above which there is a dead-end filtration, [$n = 0$ in Eq. (6)]. This critical Pe is approximated [8] by the naperian logarithm of the stability, W_d, and a threshold flux similar to the one defined in Eq. (6) can be derived:

$$j_{crit} = \frac{D}{\delta} \ln(W_d) \tag{21}$$

The theory predicts a large critical flux for particles stable in suspension and the size of which are between 0.1 to 1 μm. It then provides an explanation for the "colloidal flux anomaly" pointed out by Cohen and Probstein [2].

Another limiting case of Eq. (19) is the case where no filtration occurs, $J = 0$. The mass transport is given by calculating the limit of Sh when Pe tends to 0 in Eq. (19):

$$Sh = \frac{1}{W_d} \tag{22}$$

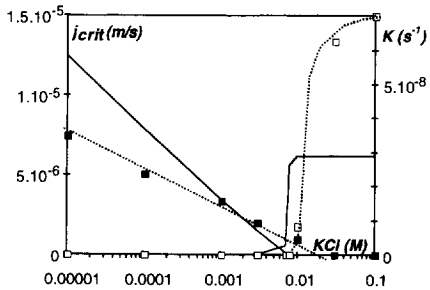

Fig. 12. Experimental j_{crit} and K versus salt concentration (dashed lines and symbols) compared to calculated (bold lines) values.

Such a relationship is similar to a one proposed by Ruckenstein and Prieve [14] describing particle deposition on a collector. Following the definition of the adhesion rate constant Eq. (2), one can derive:

$$K = \frac{S}{Vol} \frac{D}{\delta W_d} \tag{23}$$

3.3.2. Discussion

Eqs. (21) and (23) allow two experimental deposition parameters, namely the critical flux, j_{crit}, and the adhesion constant, K, to be predicted from the knowledge of the stability factor W_c (Fig. 2) using Eq. (20). These calculations for a given boundary layer thickness need to be integrated along the membrane i.e. for the whole thickness distribution. For the module and the hydrodynamic conditions used in the present study, the results of these calculations are compared to experimental results in Fig. 12. Although a quantitative agreement is not achieved between theoretical and experimental data, observed trends are predicted by the model. The decrease in surface repulsive interactions between clay particles with salt concentration explains the reduction in critical flux. On another hand, when repulsive interactions become negligible as compared to attractive ones, the appearance of an adhesion mechanism is predicted. This model describes the effects of the physico-chemical properties of the suspension on the kinetics of colloid deposition on several types of colloids, such as latex or ferric hydroxide [8]. The influence of hydrodynamic conditions seems properly represented by the model for low shear conditions (present case: outer-skinned hollow fibers with external velocity of 0.088 m/s ($Re = 1500$)) as for

larger shear hydrodynamics (inner-skinned hollow fibers with internal velocity of 1.6 m/s ($Re = 3000$) [15]). The difference between simulation and experiment can be due to the model we have taken for the surface interactions between the fouled membrane and the approaching single particle (plane to sphere system). Nonetheless, at the scale of the mechanisms considered here (a few tens of nm) nor the bentonite particle can be idealised as a sphere, neither the membrane surface is actually plane [16]. Adamczyk [17] pointed out that, in the case of the simulation of a particle collector, a good agreement between simulated and experimental data was obtained only when the surface roughness was accounted for by using a distribution function the variance of which was 30%. The present model might require such improvements before being compared quantitatively to experimental data.

4. Part II: Selectivity mechanisms

Experimental results of salt retention are now presented and discussed to conclude the salt retention by the colloids deposited on the membrane. Then, a model is developed to describe the transfer mechanism of salt through the deposit and through the boundary layer next to the deposit. Application of this model to experimental data leads to determine cake properties which are compared to those deduced from hydraulic resistance analysis (Part I). Effect of operative conditions and salt concentration on retention are discussed via the model.

4.1. Experimental results

During ultrafiltration experiments (data in Figs. 3 and 4), we observed a lower salt concentration in the permeate than in the retentate. This retention [Eq. (4)] was neither the result of the membrane as preliminary experiments showed that the membrane used did not retain the salt nor of an ion exchange mechanism as the clay was equilibrated with the salt solution a long time before ultrafiltration experiments. So, the colloid deposit on the UF membrane works as a nanofiltration membrane. This salt retention increases during an experiment and is lower when salt concentration in the suspension increases

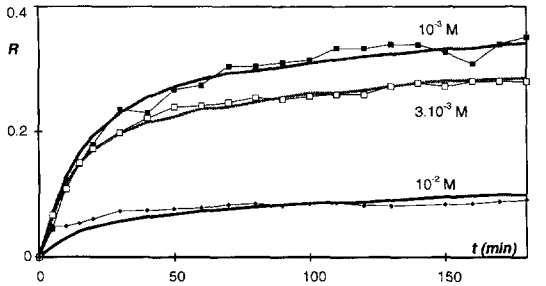

Fig. 13. Experimental salt retention versus time for data presented in Figs. 3 and 4. Symbols represent experimental data and lines calculated data.

(Fig. 13). Changes in retention can be the result of combined variations in permeation flux, in deposited mass and in salt concentration. An analysis of the influence of operating conditions on the retention is developed in the next section.

4.2. Salt retention analysis

Experimental results of salt retention leads to the development of a model for salt transport accounting for the effects of operating conditions (permeation flux and deposited mass), responsible for retention changes with time, and for the effects of surface interactions which induce the variations in retention with salt concentration.

4.2.1. Modelling

Transport in porous membranes has been described by different approaches as summarised by Opong and Zydney [18]. One of those is based on the continuity [Eq. (16)] of the mass transfer in the porous medium by convection and diffusion [Eq. (17) without term c). The boundary conditions required for integration are determined by considering one equilibrium partition coefficient, ϕ, for each side of the porous surface. The solution of this equation is very similar from relationships derived from a thermodynamic approach [19] or an electrokinetic calculation [20]. It allows the permeate concentration, c_p, to be computed from the wall concentration, c_w (Fig. 14). On the other hand, the film model describes the mass transport by convection and diffusion in the boundary layer thickness above the porous medium and allows the wall concentration to be

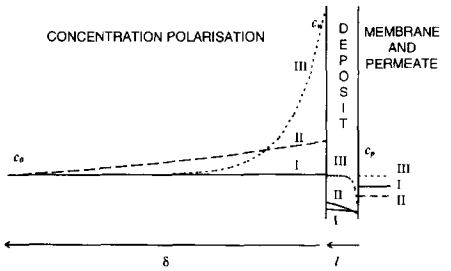

Fig. 14. Concentration profile in the boundary layer and in the cake deposit for different Pe numbers calculated with the model [Eq. (20)]. Calculations are made with value of l, ϵ and δ chosen to have $Pe_{pore} = Pe_{bl}$ and with $\phi = 0.8$.

determined from bulk concentration, c_0. The combination of these two equations allows one to calculate the observed retention R [Eq. (24)] as a function of a maximum retention coefficient, R_∞, defined as $R_\infty = 1 - \phi$. The operating conditions are accounted for through the Peclet number in the pore, Pe_{pore}, and the Peclet number in the boundary layer, Pe_{bl}:

$$R = \frac{1}{1 + \dfrac{1 - R_\infty}{R_\infty} \dfrac{e^{Pe_{bl}}}{1 - e^{-Pe_{pore}}}} \tag{24}$$

with

$$Pe_{bl} = \frac{J\delta}{D} \tag{24a}$$

and

$$Pe_{pore} = \frac{Jl}{\epsilon D} \tag{24b}$$

where l is the cake thickness and δ the mass boundary layer thickness. Pe_{bl} and Pe_{pore}, represent the non-dimensional ratio of convection to diffusion in the boundary layer and in the pore respectively.

This model can be illustrated via simplified cases with fixed parameters. For low Peclet number (small solute with large diffusion or [and] low convection) the concentration profile can be represented by case I in Fig. 14. There is negligible concentration polarisation ($Pe_{bl} < 0.1$) but an important diffusion in the porous medium leads to a dispersion and then to a poor retention. In case II (intermediate Peclet number), there is a low polarisation and a low dispersion in the porous medium leading to large solute retention. In case III where Peclet number is large, there is a negligible dispersion by diffusion in the porous medium ($Pe_{pore} > 5$) but an important concentration polarisation which induces a low retention. Such a model has been used by Opong and Zydney [18] to explain the maximum value found when plotting retention versus permeate flux in bovine serum albumin ultrafiltration.

The partition coefficient, ϕ, not affected by steric hindrance for small solutes such as salts, can be written by considering a Boltzman distribution of solute concentration versus the electrostatic potential [21] between two plates:

$$\phi = 1 - R_\infty = \frac{2}{d_i} \int_0^{d_i} e^{-\frac{V}{kT}} dx \tag{25}$$

A series of equations allows us to model the salt retention with only one parameter to describe the cake: the interparticle distance d_i. The distance d_i is used to calculate the partition coefficient [Eq. (25)] and the cake porosity [Eq. (9)]. The experimental data for the deposited mass is used to determine the deposit thickness [Eq. (8)] and then the Pe_{pore} [Eq. (24b)]. Therefore one can calculate the salt retention with Eq. (24). Reciprocal solution of this system of equations leads us to deduce, from experimental data of filtration (Figs. 3 and 4), the interparticle distance explaining the retention shown in Fig. 13.

4.2.2. Discussion

Best fitted values of d_i are shown in Fig. 15. We observe that salt retention analysis predicts that the interparticle distance passes through a minimum. As can be seen in this figure, the results (symbols) are consistent with those obtained from hydraulic resis-

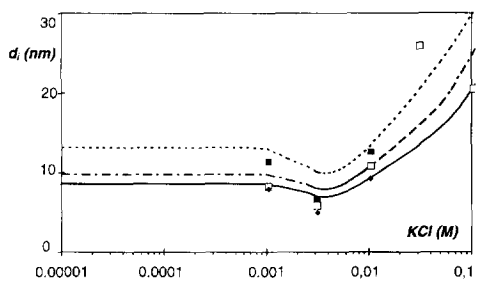

Fig. 15. Interparticle distance calculation, d_i, from salt retention analysis (■ = 50 kPa, □ = 100 kPa, ◆ = 150 kPa) compared with d_i, calculated from hydraulic resistance analysis (- - - = 50 kPa, — — — = 100 kPa, ——— = 150 kPa).

tance analysis (lines) and with data calculated from theoretical considerations (Fig. 10). An important result is that the salt retention and hydraulic resistance can be described by the same variation in the interparticle distance in the cake. This result supports the different approaches proposed above for the transport of water and of salt through the cake. A peculiar importance is then given to the interparticle distance which characterises the resistance to the solvent (hydraulic resistance) as well as the resistance to the salt transport (salt retention).

Effects of the ionic concentration on retention are analyzed in Fig. 16. This figure represents the maximum retention coefficient, R_∞, (by definition independent of operating conditions) versus salt concentration. The maximum retention is found to be very sensitive to the salt concentration during experiments (symbols in Fig. 16). Theses variations are compared to maximum retention calculated for a given interparticle distance (dotted lines in Fig. 16). These curves show the effect of salt concentration on the maximum retention coefficient: when salt concentration increases, repulsive interactions between an ion and the deposit of charged particles decrease leading to a lower retention. Deviations of experimental trends from these curves are due to the change in interparticle distance with salt concentration (Fig. 15). The maximum retention (or the partition coefficient), which is an intrinsic property of the selective layer, is the result of a combination of the variation in interparticle distance (acting as the pore size of a nanofiltration membrane) and of the variation in the repulsive interaction versus salt concentration (DLVO theory).

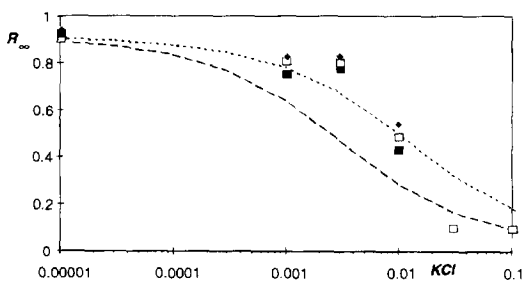

Fig. 16. Variation of the maximum retention versus salt concentration deduced salt retention analysis (■ = 50 kPa, □ = 100 kPa, ◆ = 150 kPa). Dotted lines corresponds to maximum retention calculated with Eq. (21) for a given interparticle distance (--- d_i = 10 nm, ——— ——— d_i = 20 nm).

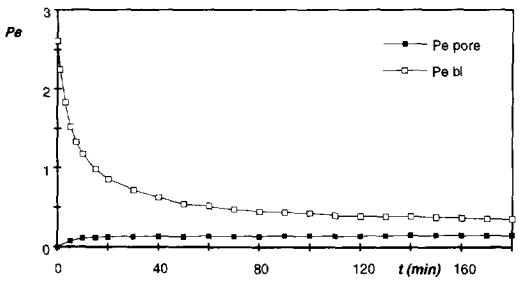

Fig. 17. Variation in the Pe_{pore} and the Pe_{bl} against time deduced from modelling.

Effects of operating conditions on salt retention can be seen in Fig. 17 where calculated Pe_{pore} and Pe_{bl} are plotted against time for a given experiment. Analysis of these two numbers allows us to determine the relative influence of the transport by convection and by diffusion in the boundary layer and in the pores. The factor limiting the selectivity and the place where it takes place can be deduced from such an analysis. One can see that Pe_{pore} remains almost constant during our experiments. This is due to the fact that for our conditions (retention by a cake growing in thickness) the product Jl is almost constant (J is reduced because the thickness of the cake, l, increases). The increase in salt retention during the experiments is then essentially explained by the decrease in Pe_{bl} and then in concentration polarisation when permeation flux is reduced. However, application of the film model alone would lead to a mistake. Pe_{pore} in Fig. 17 is low and quite smaller than 5 (value above which the transport in the pore is not limiting). So the salt retention is reduced by dispersion in the porous medium. Application of the film model would lead to determine a retention factor smaller than the maximum retention deduced from the full model and then to an important error on the interparticle distance. Our experiments are then an example of salt retention both controlled by concentration polarisation (large Pe_{bl}) and by dispersion in the pore (low Pe_{pore}).

It is interesting to compare the mechanism of salt retention by a colloid deposit on an ultrafiltration membrane with nanofiltration membranes which are developed to partially retain salts. A typical operat-

Table 1
Comparison of salt retention by a nanofiltration membrane (Filmtec NF40) and a clay deposit on an ultrafiltration membrane

	J (m/s)	ΔP (kPa)	KCl (M)	R
NF 40, Filmtec [21]	1×10^{-6}	1000	3×10^{-2}	0.45
Clay deposit on an ultrafiltration membrane	1×10^{-6}	100	3×10^{-3}	0.25

ing condition of a Filmtec NF 40 [22] and results of salt retention of the present work are listed in Table 1. One can see that with nanofiltration membranes salt retention is better and still important for high salt concentration. But, on the other hand nanofiltration membranes are much less permeable and need, in order to have an equivalent permeation flux, a pressure ten times larger than that required with a colloid deposit. Deposit of clay on an ultrafiltration membrane can then be an alternative solution when processing liquids with low salt concentration to remove, e.g. nitrate in potable water. Moreover, such a solution requires only a reversible change of an existing ultrafiltration unit and then can be used only when retention of salt is needed.

5. Conclusion

In this paper, the influence of surface interactions on colloid filtration have been investigated through the study of three transfer mechanisms: transfer of colloid from the bulk to the membrane (deposition) and transfer of water (hydraulic resistance) and of

Table 2
Synthesis of variations of transfer mechanisms with salt concentration: (A) mass transfer of a particle from the bulk to the deposit, (B) water transfer through the deposit and (C) salt transfer through the deposit. Phenomena implied in these variations are in bold

			Salt concentration	10^{-5} M	10^{-2} M c.c.c.	1 M
			Stability of the suspension	↘	1	<1
A	*Deposition kinetics*	Critical flux		↘ **interaction induced migration**	0	0
		Adhesion constant		0	0	↗ **adhesion**
B	*Hydraulic resistivity of the deposit*			↗ **cake contraction**	Max	↘ **coagulation**
A+B	Productivity			↘	Min	↗
C	*Selectivity* Maximum retention			↘ **cake contraction**		↘ **coagulation**
				& reduction of repulsive interaction solute-cake		

salt (salt retention) through the colloid deposit. This work is based on ultrafiltration experiments of a clay suspension (Bentonite) with different salinities and then different surface interactions. Experimental variations in transfer mechanisms deduced from these experiments and major phenomena involved are summarised in Table 2.

Analysis of fouling kinetics (mass transfer from the bulk to the deposit) at low ionic strength reveals a high critical permeate flux and an adhesion mechanism for salt concentrations larger than the critical concentration of coagulation. Mass deposition is theoretically described as the result of particle transport by convection, diffusion and interaction induced migration in a mass boundary layer surrounding the surface. For large repulsive interaction, a limit of the mass transfer equation derived from this analysis, leads to the definition of a critical flux (flux below which no fouling should theoretically occurs) depending on the suspension stability. This relationship predicts the decrease of the critical flux by a reduction in the interaction induced migration. So, for salt concentrations larger than ccc, this critical flux is zero because of no repulsive interaction: all the mass brought by convection is deposited as in dead-end filtration. Another limit of the transfer equation for non-filtration describes the adhesion mechanism when an attractive interaction exists.

The hydraulic resistance (transfer of water through the deposit) variations with salt concentration present a maximum. A balance between surface interaction forces and drag convection force on particles of the cake determine the cake porosity. When combined to the effect of salt concentration to the particle size, this leads to the description of the hydraulic resistance of the cake through a modified Kozeny–Carman relationship. The maximum of hydraulic resistance is explained as the fact that, for salt concentration near the ccc, the repulsive interactions are not strong enough to stand the drag convection force in the cake, which leads to cake packing, but on another hand, surface interaction are still large enough to prevent particle from coagulation which would improve the cake permeability.

Salt retention mechanisms by the fouling layer are based on a partition created by repulsive interactions between an ion and the charge on the deposit. A partition coefficient is deduced from experimental retention, after accounting for effects of concentration polarisation and of dispersion through the cake. Salt retention by the colloidal deposit (salt transfer through the deposit) is a complex combination of the cake geometry and of the operating conditions (permeation flux, deposited mass and salt concentration). The partition coefficient, an intrinsic parameter of the deposit selectivity, can be deduced from observed retention via a model of salt transport by diffusion and convection in the boundary layer (concentration polarisation) and in the deposit (dispersion). This coefficient depends on the cake geometry and on the repulsive interaction between an ion and the charge of the deposit. As can be seen in Table 2, for salt concentration lower than ccc, the maximum retention is almost constant: the negative effects of the decrease in repulsive interaction are balanced by the benefits of the increase in cake resistance caused by the cake contraction. Then, for concentration larger than the ccc, the maximum retention is quickly reduced to zero by the combined effect of the decrease in interaction and the lower resistance of the cake. Analysis of these results through a model for the maximum retention leads to the conclusion of a cake geometry similar to the one deduced from the hydraulic resistance analysis. Compared to nanofiltration processes, retention of salt by a colloid deposit on an ultrafiltration membrane represents an interesting way to remove salt from low concentration solutions.

When colloids are present in a fluid the stability seems then to be an essential parameter to estimate the effects of those colloids on the filtration process. A low positive stability induces a minimal productivity of the process: low porosity for the cake, no limitation of the deposition (critical flux close to zero) and no enhanced permeability by coagulation. Moreover, the knowledge of the stability can help in the choice of operating conditions. For example the cross-flow efficiency to prevent colloidal fouling is directly linked to the stability: experiments have shown that cross-flow is useless when processing with destabilised colloidal suspensions.

6. List of symbols

a	particle radius (L)
D	diffusion coefficient ($L^2\ T^{-1}$)

c	concentration ($M\ L^{-3}$)
d_i	interparticle separation distance in the cake (L)
e	bentonite particle thickness (L)
J	permeate flux ($L\ T^{-1}$)
j_{crit}	critical permeate flux ($L\ T^{-1}$)
k	Boltzmann constant ($M\ L^2\ T^{-2}\ K^{-1}$)
K	adhesion rate (T^{-1})
l	cake thickness (L)
M_d	deposited mass of particle per unit of membrane area ($M\ L^{-2}$)
N	mass flux ($M\ L^{-2}\ T^{-1}$)
P	pressure ($M\ L^{-1}\ T^{-2}$)
R	salt retention rate
R_∞	maximum retention rate
R_m	hydraulic resistance of the membrane (L^{-1})
R_c	hydraulic resistance of the fouling layer (L^{-1})
Pe_{bl}	Peclet number (ratio convection/diffusion) for the boundary layer
Pe_{pore}	Peclet number (ratio convection/diffusion) for the porous media
S	membrane area (L^2)
Sh	Sherwood number: ratio mass transfer/diffusion
t	time (T)
V	total interaction energy ($M\ L^{+2}\ T^{-2}$)
Vol	suspension volume (L^3)
W_d	stability factor with respect to deposition
W_c	stability factor for coagulation

6.1. Greek symbols

α	specific hydraulic resistance ($L\ M^{-1}$)
δ	mass transport boundary layer thickness (L)
ϵ	porous medium porosity
ϕ	partition coefficient
μ	suspension viscosity ($M\ L^{-1}\ T^{-1}$)
ρ_s	density of the particles ($M\ L^{-3}$)

Acknowledgements

Special thanks to J.P. Lafaille for technical assistance and to Lyonnaise des Eaux and CNRS for supporting this work through GdR no. 109.

References

[1] G. Belfort, R.H. Davies and A.L. Zydney, The behaviour of suspensions and macromolecular solutions in crossflow microfiltration, J. Membrane Sci., 96 (1994) 1–58.

[2] R.D. Cohen and R.F. Probstein, Colloidal fouling of reverse osmosis membranes, J. Colloid Interf. Sci., 114 (1986) 1.

[3] R.M. McDonogh, C.J.D. Fell and A.G. Fane, Surface charge and permeability in the ultrafiltration of non-flocculating colloids, J. Membrane Sci., 21 (1984) 285–294.

[4] C. Causserand, Etude des mécanismes de sélectivité d'une membrane d'ultrafiltration, Thèse de l'Université Paul Sabatier, Toulouse, France, 1992.

[5] C. Gourgues, P. Aimar and V. Sanchez, Ultrafiltration of bentonite suspensions with hollow fiber membranes, J. Membrane Sci., 74 (1992) 51–69.

[6] A. Delgado, F. Gonzalez-Caballero and J.M. Bruque, On the zeta potential and surface charge density of montmorillonite in aqueous electrolyte solutions, J. Colloid Interf. Sci, 113 (1986) 1.

[7] E.J.W. Verwey and J.TH.G. Overbeek, Theory of the Stability of Lyophobic Colloids: The Interaction of Sol Particles Having an Electric Double Layer, Elsevier, New York, 1948.

[8] P. Bacchin, P. Aimar and V. Sanchez, Model for colloidal fouling of ultrafiltration membranes, AIChE J., 41(2) (1995) 368–376.

[9] H. Tamai and T. Suzawa, Latex deposition on fibers: Effect of electrolytes on rate and interaction energy, J. Colloid Interf. Sci., 88 (1982) 2.

[10] A.D. Scheidegger, The Physics of Flow Through Porous Media, 3rd edn., University of Toronto Press, 1974, p. 158.

[11] K. Norrish, The swelling of montmorillonite, Discuss. Faraday Soc., 18 (1954) 20.

[12] T.G.M. Van de Ven, Effects of electrolytes, polymers and polyelectrolytes on particle deposition and detachment, Colloids Surf., 39 (1989) 107–126.

[13] X. Jia and R.A. Williams, Particle deposition at a charged solid/liquid interface, Chem. Eng. Commun., 91 (1990) 127–198.

[14] E. Buckenstein and D.C. Prieve, Rate of deposition of Brownian particles under the action of London and double layer forces, J. Chem. Soc., Faraday Trans. 2, 69 (1973) 1522.

[15] H. De Balmann, Utilisation de l'ultrafiltration dans le traitement de l'eau, Thèse de l'Université Paul Sabatier, Toulouse, France, 1988.

[16] A. Bessieres, Etude des propriétés fonctionnelles et structurales de membranes synthétiques par rétention de molécules calibrées et microscopie à champ proche, Thèse de l'Université Paul Sabatier, Toulouse, France, 1994.

[17] Z. Adamczyk, Particle deposition from flowing suspensions, Colloids Surf., 39 (1989) 1–37.

[18] W.S. Opong and A.L. Zydney, Diffusive and convective protein transport through asymmetric membranes, AIChE J., 37 (1991) 10.

[19] K.S. Spiegler and O. Kedem, Thermodynamics of hyperfil-

tration (reverse osmosis): criteria for efficient membranes, Desalination, 1 (1966) 311–326.

[20] G. Jacazio, R.F. Probstein, A.A. Sonin and D. Yung, Electrokinetic salt rejection in hyperfiltration through porous materials. Theory and experiment, J. Phys. Chem., 76(26) (1972) 4015–4023.

[21] H. Brenner and L.J. Gaydos, The constrained Brownian movement of spherical particles in cylindrical pores of comparable radius, J. Colloid Interf. Sci., 57 (1977).

[22] R. Rautenbach R. and A. Groschl, Separation potential of nanofiltration membranes, Desalination, 77 (1990) 73–84.